

Mechanism of Interaction of Water above the Methylammonium Lead Iodide Perovskite Nanocluster: Size Effect and Water-Induced Defective States

Jie Huang, Bowen Wang, Hejin Yan, and Yongqing Cai*



Cite This: *J. Phys. Chem. Lett.* 2024, 15, 575–582



Read Online

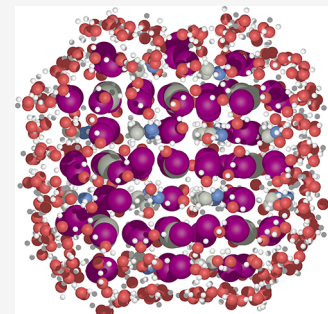
ACCESS |

Metrics & More

Article Recommendations

Supporting Information

ABSTRACT: Water is often viewed as detrimental to organic halide perovskite stability. However, evidence highlights its efficacy as a solvent during organic perovskite liquid synthesis. This paradox prompts an investigation into water's influence on perovskite nanoclusters. Employing first principle calculations and *ab initio* molecular dynamics simulations, surprisingly, we discover some subsurface layers of methylammonium lead iodide (MAPbI_3) nanoclusters exhibit stronger relaxation than surface layers. Moreover, a strong quantum confinement effect enhances the band gap of MAPbI_3 as the nanocluster size decreases. Notably, the water molecules above MAPbI_3 nanoclusters induce rich localized defect states, generating low-lying shallow states above the valence band for the small amounts of surface water molecules and band-like deep states across the whole gap for large nanoclusters. This work provides insights into water's role in the electronic structure and structural evolution of perovskite nanoclusters, aiding the design of water-resistant layers to protect perovskite quantum dots from ambient humidity.



Hybrid organic-inorganic perovskites (HOIPs) stand out as the most promising materials for next-generation solar cells due to their combination of low cost, high efficiency, easily tunable bandgap, extensive exciton diffusion length, and remarkable charge-carrier mobility.^{1–8} A HOIP follows the formula ABX_3 , where A represents an organic cation, B denotes a metal cation (i.e., Pb and Sn), and X signifies an anion (halogen). Among all the HOIP materials, methylammonium lead iodide MAPbI_3 perovskite, where MA denotes CH_3NH_3^+ , has attracted significant attention because of its exceptional light-absorbing characteristics.

Unfortunately, HOIPs such as MAPbI_3 suffer from the issue of instability which presents a significant challenge that constrains the applications.^{4,5,8} Exposure to environmental molecules, i.e., moisture and oxygen, induces the degradation of the structure. Under working conditions, the presence of heat and light irradiation would deteriorate the situation and accelerate the degradation.^{9–12} In particular, water, highly likely to be introduced during synthesis, storage, and serving processes, poses a significant effect on the stability and performance of perovskite materials.^{13–16} Subjecting MAPbI_3 solar cells to relative humidity levels exceeding 55% rapidly impairs device performance.^{17–21} Consequently, maintaining the long-term stability of the MAPbI_3 perovskite structure in moist conditions has become a central focus of research.^{22–25}

Ironically, water can be intentionally introduced for growing HOIPs in the solution-based synthesis method of MAPbI_3 ,^{26,27} thus a dual role is made by water. As the most clean and nontoxic solvent, water was found to be a promising solvent or cosolvent to make a homogeneous precursor solution.^{28,29}

During the formation and crystallization of MAPbI_3 , proper control of moisture has been found to modulate the thin film morphology and improve the performance of solar cells.^{13,30–37} In contrast to other solvents commonly used for perovskite precursors, water does not fit neatly into the category of strongly coordinating solvents for lead ions due to its limited capacity to solvate PbI_2 and its moderate donor number.²⁷ Nevertheless, the high polarity of water molecules makes it challenging to produce iodide-rich iodoplumbates.²⁷ How water would affect the structure and properties of MAPbI_3 remains elusive, especially for those seeding MAPbI_3 nanoclusters. The adsorbing behavior of water on perovskite nanoclusters remains an open question.

In this work, aiming at uncovering the effect of water, we perform density functional theory (DFT) calculations on MAPbI_3 clusters. By tracking the variation of structures with *ab initio* molecular dynamics (AIMD) simulations, we provide nanoscale mechanisms of bond distortion and relaxation upon the uptake of water molecules. Moreover, we also examine the quantum size effect on band gaps of MAPbI_3 nanoclusters and explore how water affects the electronic properties, i.e., identifying any defective states arising from water adsorption. Our work provides insight into the impact of water at the

Received: October 9, 2023

Revised: January 3, 2024

Accepted: January 8, 2024

Published: January 10, 2024



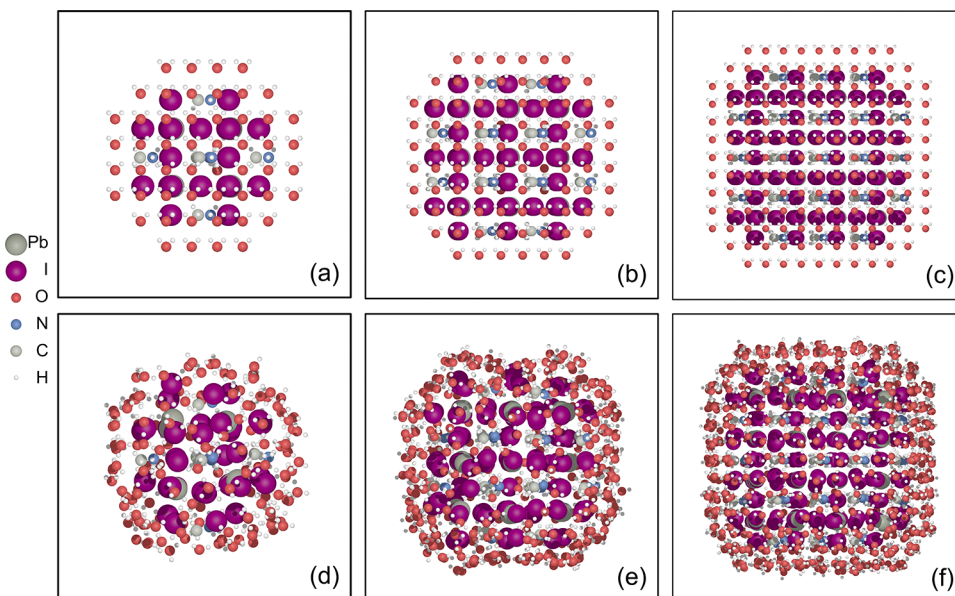


Figure 1. Initial (a, b, c) and corresponding relaxed (d, e, f) configurations of three different sized MAPbI_3 nanoclusters surrounded by a layer of water molecules.

microscopic level on the structure of MAPbI_3 clusters and holds immense potential for enhancing our understanding of degradation mechanisms and for future optimization of HOIPs.

Three different-sized nanoclusters, $\text{MA}_7\text{Pb}_8\text{I}_{36}$, $\text{MA}_{32}\text{Pb}_{27}\text{I}_{108}$, and $\text{MA}_{81}\text{Pb}_{64}\text{I}_{240}$, with sizes of 1.50, 2.13, and 2.76 nm, respectively, were constructed by using Atomic Simulation Environment (ASE).^{38,39} For convenience, we refer to these nanoclusters as small, middle, and large, respectively. Initial atomic configurations for the three systems are shown in Figure 1a–c, with the nanoclusters built from the relaxed bulk MAPbI_3 structure. For each case, a monolayer of water molecules was placed surrounding nanoclusters, with 156, 370, and 891 water molecules for the small, middle, and large systems, respectively. Water molecules are evenly distributed on the grids based on the density of bulk water at 300 K. The minimum distance between the oxygen atoms in water molecules and the atoms of MAPbI_3 nanoclusters was set to 2.5 Å. A vacuum layer with a thickness of 5.5 Å was inserted to avoid the interaction between images of the nanoclusters under periodic boundary conditions. The optimized configurations for the three systems are shown in Figure 1d–f. The simulation settings and adsorption energies are detailed in Table 1.

DFT calculations and AIMD simulations were conducted using CP2K/QUICKSTEP,⁴⁰ employing Goedecker–Teter–Hutter (GTH) pseudopotentials^{41,42} with single-zeta sets (SZV-MOLOPT-GTH for C, N, O, and H; SZV-MOLOPT-SR-GTH for Pb and I), the Perdew–Burke–Ernzerhof (PBE) functional,⁴³ and DFT-D3 correction⁴⁴ for the dispersion interaction. The Broyden–Fletcher–Goldfarb–Shanno (BFGS)^{45–48} optimizer is employed for small and midsized systems, while the Limited-memory BFGS (L-BFGS)⁴⁹ optimizer is utilized for the large system. AIMD simulations were performed with canonical NVT ensembles with a Nosé–Hoover⁵⁰ thermostat at 300 K for 12 ps using a time step of 1 fs. And MDAnalysis^{51,52} was used to analyze AIMD trajectories.

As shown in Figure 1, in comparison to the initial structures, optimized MAPbI_3 clusters covered by water exhibit a certain

Table 1. Simulation Settings: the Cluster Sizes, Water Molecule Numbers, Adsorption Energies in Units Atomic Unit of Energy (a.u.), Highest Occupied Molecular Orbitals (HOMOs), Lowest Unoccupied Molecular Orbitals (LUMOs), and Band Gaps of the Naked MAPbI_3 Nanoclusters^a

	Small	Middle	Large
Cluster	$\text{MA}_7\text{Pb}_8\text{I}_{36}$	$\text{MA}_{32}\text{Pb}_{27}\text{I}_{108}$	$\text{MA}_{81}\text{Pb}_{64}\text{I}_{240}$
Cluster size (nm)	1.50	2.13	2.76
H_2O number	156	370	891
Atom number	568	1501	3625
Box volume (nm ³)	30.04	49.13	90.74
E_{adsorb} per H_2O (a.u.)	-0.0174	-0.0131	-0.0100
HOMO (eV)	0.593	0.113	0.582
LUMO (eV)	2.565	1.815	1.065
Band gap (eV)	1.972	1.702	0.484

^aThe cluster sizes were obtained by averaging the diameters in three directions. The adsorption energies were calculated by $E_{\text{adsorb}} = E_{\text{total}} - E_{\text{cluster}} - E_{\text{water}}$ where E_{total} , E_{cluster} , and E_{water} are energies of the relaxed configuration of nanocluster and water, naked nanocluster, and water clusters, respectively. For further details regarding the adsorption energy calculations, please refer to Table S1 in the Support Information (SI).

degree of expansion. However, the extent of expansions is limited, essentially largely maintaining clusters' octahedral structures. The surface water in the outer layer of the optimized structure forms a hydrogen bonding network that evenly envelops the clusters. (Figure S5 in SI shows the hydrogen bonding network.) We are particularly interested in the structural changes of MAPbI_3 after the introduction of the water layer, in other words, geometrical modifications of bonds before and after relaxation. We thus monitor the distribution of the Pb–I distance.

In Figure 2, the three subplots (a), (b), and (c) show the distributions of Pb–I distance of the unrelaxed and relaxed structures for the three clusters. As can be seen from Figure 2, for the three cases directly cut from bulk MAPbI_3 (the unrelaxed cases), the Pb–I bond distributes quite narrowly

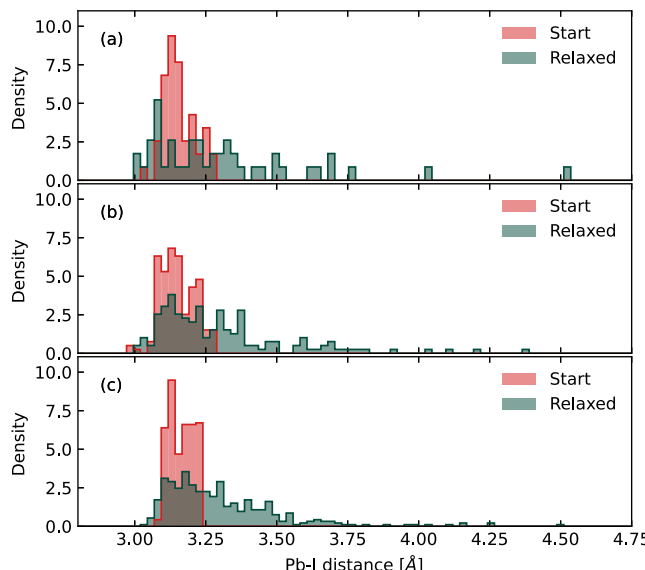


Figure 2. Pb–I distance distributions before and after relaxation for small (a), middle (b), and large (c) nanoclusters. The vertical axis indicates the probability density, which is defined as $\rho_i = n_i/(ND_i)$, where n_i is the number of Pb–I distances in the i -th bin range, N is the total number of counted distances, and D_i is the width of the i -th bin. The area under the histogram integrates to 1, i.e., $\sum \rho_i D_i = 1$.

with peaks at around 3.15 Å, ranging from 3 to 3.25 Å. However, after relaxation, the peak broadens significantly and the values of Pb–I bond length extend from around 3.00 to 4.50 Å. This reflects a strong relaxation and distortion of the perovskite units upon forming nanoclusters. The presence of long Pb–I bonds greater than 4 Å indicates the presence of significant stress and strain inside these structures. We also find that the smaller the nanocluster the higher the population of those elongated Pb–I bonds. The broadened peaks of the Pb–I distance distributions suggest the presence of an elongated and stretched lattice surrounding the Pb atoms. We can identify discrete peaks in the extending distribution of Pb–I bonds, specifically within the Pb–I distance range of 3.0 to 3.5 Å, indicating the presence of the shell-like elongated lattice surrounding the center.

To provide further spatial dependence of the relaxation from the surface to the center, we analyze the variation of the Pb–I distance for all of the Pb–I bonds before and after relaxation. As shown in Figure 3, the radial positions of all the I atoms, with their coordinates relative to the mass center of the cluster, are depicted together with the change of bond length, $\Delta \text{Pb–I}_{\text{dis}}$. A positive (negative) value indicates that the bond is stretched (compressed). The probability densities for the distribution of the change in Pb–I distance are also plotted on the right side of these plots in Figure 3.

In all three sizes, the average values (dashed lines) of change in the Pb–I distance are positive, indicating that more than half of the Pb–I bonds in the nanocluster are stretched compared to the bulk phase. Squeezed Pb–I bonds are also detected in each shell defined by the iodine atoms. The coexistence of elongated and compressed Pb–I bonds shows a strong Jahn–Teller distortion⁵³ of the octahedral structures. Interestingly, the most significant relaxation in middle and large systems does not occur in the outermost layer, as usually assumed in the bulk surface, which interacts directly with the water molecules. Instead, the strongest bond elongation is

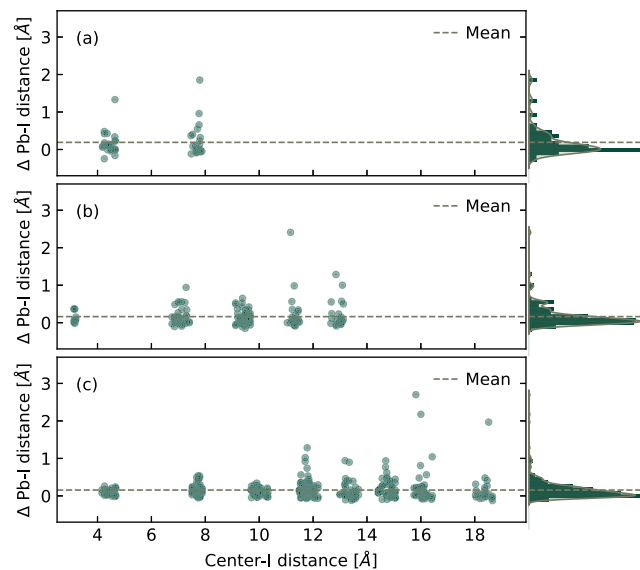


Figure 3. Spatially resolved distribution of the change in Pb–I distance for small (a), middle (b), and large (c) nanoclusters. The horizontal axis is the position of the I atom from the mass center of the corresponding nanocluster. The dashed lines correspond to the average values of the change in the Pb–I distance.

found in the subsurface layers, extending to four iodine subsurface layers. This finding suggests that the outermost layer serves as chemical passivation and is water resistant, while the subsurface layers, with the most bond relaxation, undergo severe bond stretching. The outermost passivation layer, subjected to lattice discontinuity, largely maintains the octahedral lattice of the nanoclusters while resisting the water, as illustrated in Figure S1, fourth column, in the SI. In contrast, the interior atoms close to the center tend to deviate slightly from their bulk positions. As the MAPbI₃ size increases, the change in Pb–I distance of the innermost layers decreases from the range [-0.28, 1.34] to [-0.02, 0.28], which indicates that the inner structure of a larger MAPbI₃ nanocluster is much harder to disturb compared to a small one. Therefore, presumably, the loose subsurface structures are the origins of structural instability. How to effectively stabilize them is the key to promoting the population of seeds and the growth of high-quality nanoclusters.

To better understand the effects of water molecules on MAPbI₃ clusters, we explored the perovskite–water ratio impact on the structure of the MAPbI₃ cluster. Starting from a system like Figure 1a, we systematically reduced the number of surrounding water molecules from 156 to 0. For further details regarding the effect of the perovskite–water ratio, please refer to Figure S1 and Table S2 in the SI. Through our calculations, we notice that the small nanocluster would lose its octahedron structure during the structural relaxation process if there are no surrounding water molecules, while the basic crystal structure was preserved for the same nanocluster but with a small amount of water molecules. (Please refer to Figure S2 in the SI for the structure optimization processes of both systems.) Hence, water molecules surrounding nanoclusters play a certain role in stabilizing the Pb–I lattice and promoting the probability of seeding of the nanoclusters.

We next examined the size-dependent electronic property of MAPbI₃ nanoclusters and the role of the water layer adsorbed around the surface. We attempt to answer the following

questions. First, how does the band gap of MAPbI₃ nanoclusters evolve with the size? Second, what is the effect of the surface water layer on the band gap? Are there any water-induced defect states? The projected density of states (PDOS) of the intrinsic nanoclusters, i.e., the structure without the surrounding water molecules, is shown in Figure 4. As the

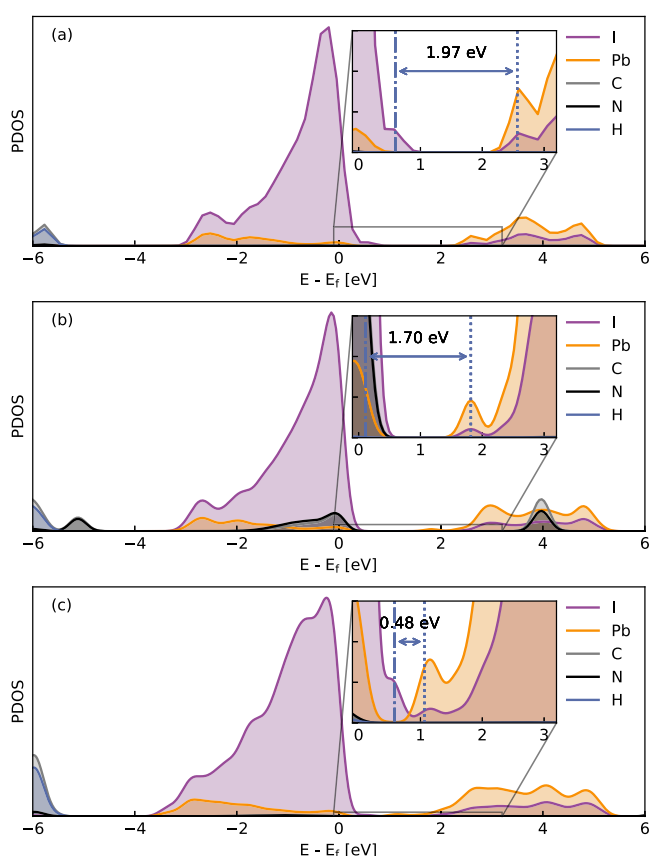


Figure 4. PDOS of the relaxed MAPbI₃ clusters without adsorbing water molecules on the surface with small (a), middle (b), and large (c) sizes. The band gaps are 1.97, 1.70, and 0.48 eV, respectively.

size of the nanocluster increases from 1.50 to 2.76 nm, the band gap decreases from 1.97 to 0.48 eV, consistent with the quantum confinement effect. The spatial confinement of the electrons and holes in small nanoclusters results in an increase in the energy spacing between the valence and conduction bands. The details of the highest occupied molecular orbital (HOMO) and the lowest unoccupied molecular orbital (LUMO) are given in Table 1. Notably, there exists a strong drop of the band gap from 1.70 eV for MA₃₂Pb₂₇I₁₀₈ to 0.48 eV for MA₈₁Pb₆₄I₂₄₀. This would arise from an improved stabilization of the octohedral unit at the inner core, as shown in Figure 2, with the atomic arrangement being more similar to the bulk lattice. It seems that the size of MA₈₁Pb₆₄I₂₄₀ would be a critical value for becoming a bulk-like nanocluster. In addition, for all the intrinsic nanoclusters, there is no defective state in the gap regardless of their high surface ratio, rich surface dangling atoms, and strong distortion of bonds, indicating a good defect tolerance of MAPbI₃.

With the addition of water molecules above the cluster surface, defective states formed within the band gap of MAPbI₃. The introduction of water molecules results in the emergence of defect states in the MAPbI₃ nanoclusters. By

comparing the PDOS plots of nanoclusters without water molecules (Figure 4) and with water molecules (Figure 5), we

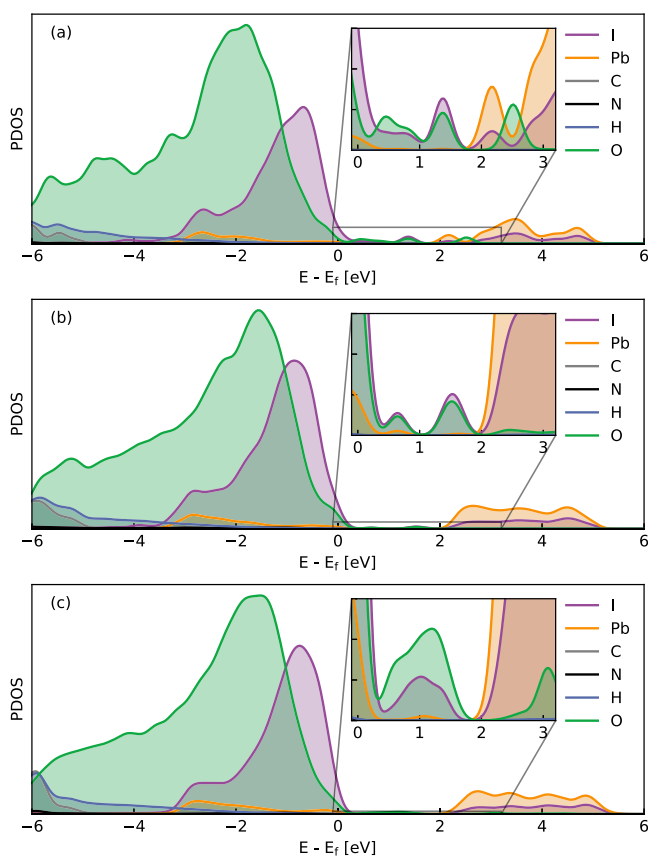


Figure 5. PDOS plots for the relaxed MAPbI₃ clusters including water molecules in small (a), middle (b), and large (c) sizes. Defect densities of states can be found in all systems. We can observe that the most significant contributions to the defect density of states come from the atoms of the O and I atoms.

find even for the smallest perovskite there are water-related states lying above the valence band top of MAPbI₃. PDOS analysis shows that those states are mainly comprised of water and iodine. The strong overlapping of both states suggests a clear resonance of the water and surface iodine species and an overlapping of water and iodine orbitals.

The effect becomes particularly pronounced when a significant number of water molecules come into contact with the nanoclusters, which occurs with a higher concentration of water molecules. Notably, the width of these water-induced states increases with the size of the nanocluster or equivalently with the surface area of the water layer. The low-lying states formed in the small nanocluster, narrow and shallow above the valence band, now broaden into band-like states across the whole band gap in the big nanocluster. The size-dependent behavior of the defective state suggests its origin from H₂O molecule rather than the distortion of octohedra of Pb—I backbone. The low-lying shallow state above the valence band further indicates that each adsorbed H₂O molecule acts as a p-type dopant, taking electrons from MAPbI₃. In ultraviolet photoelectron spectroscopy (UPS) experiments, it was reported that the spectrum of MAPbI₃ shows a blue shift after the sample is exposed to water.⁵⁴ The experimental findings align well with the situation in which I atoms bind with water and lose electrons. This result suggests

that water plays a crucial role in the electronic properties of MAPbI_3 clusters by affecting their density of states and carriers concentration. It is noteworthy that the presence and relative position of such defective levels are less likely to be changed with the inclusion of spin–orbital coupling in the calculation, which, however, is not included here.

Therefore, besides the well-known degradation, water molecules above MAPbI_3 nanoclusters can cause severe outcomes, including a negative impact on the efficiency of solar cells. A narrower band gap reduces the amount of energy that can be harvested from the solar spectrum, resulting in a lower energy conversion efficiency for the solar cell. These water-induced defective states, even the low-lying shallow states for a tiny content of water molecules, would quench light emission or reduce the absorption. Any residual water molecules left above the surface can also cause band bending of the perovskite materials, inducing a hysteresis of the light response and utilization.

In order to investigate the dynamic behavior of MAPbI_3 nanoclusters in water, AIMD simulations at 300 K were conducted for the small nanocluster. The simulation settings, including cluster size, number of water molecules, and box volume, are shown in Table 1. The radial distribution functions (RDFs) were calculated to provide insight into the dissolution process. In Figure 6a, the RDFs for Pb–I are plotted for each time window with a length of 2 ps. In the first time window starting at 0 ps, there are clear maximum values around 3, 7, and 9 Å, indicating that the nanocluster remains in a periodic lattice structure. However, the peaks become broadened and even eventually disappear with time, suggesting that the periodic lattice structure is destroyed, i.e., within the first 4 ps.

The RDFs for N–I and N–O were also calculated. In Figure 6b, the first peak of RDF $g_{\text{NI}}(r)$ is in a downward trend, indicating that an increasing number of MA cations are leaving their original positions and contributing to the dissolution of the nanocluster. Conversely, Figure 6c shows that the first peak of RDF $g_{\text{NO}}(r)$ increases over time, indicating that water molecules capture MA cations during the dissolution process. RDFs show significant changes in the structure of the nanocluster occur in the first 4 ps.

In Figure 7, we present a series of plots that showcase the dynamic evolution of the MAPbI_3 nanocluster configuration, topological connection of Pb–I bonds, degree distribution, and I–Pb–I angle distribution over time. The topological connection graph is generated based on the geometric criterion that the Pb–I distance is less than 3.4 Å. In the plotted graphs, the purple and gray nodes represent I and Pb atoms, respectively.

Our observations indicate that the degree of Pb nodes, which signifies the number of I atoms bonded to them, decreases with time. At 64 fs, there are 8 Pb nodes with degrees of 6, indicating that each of them is bonded with 6 I atoms. However, at 1024 fs, no Pb node has a degree of 6, indicating the absence of any regular octahedron formation via the Pb and I atoms. It is worth mentioning that the newly formed Pb–I bonds are not considered in these graph plots as we only focus on the impact of water on the nanocluster's structural integrity. Additionally, the distribution of angle I–Pb–I at 64 fs shows that most of the angles are around 90°, which is similar to the crystal structure of MAPbI_3 . However, at 2048 fs, the I–Pb–I angle distribution is vastly different from that at 64 fs. Besides, calculations of the structural similarity between the configurations at time 0 and time t in AIMD trajectories for both the small nanocluster in the water layer and bulk water (Figure S3 in SI) also indicate that the crystal structure of the small nanocluster is severely damaged within just about 2 ps. As shown in Figure S4 in the SI, we also calculated the coordination numbers for N–O, N–I, Pb–N, and Pb–I and found substantial changes in all four coordination numbers in the first 2 ps, indicating significant alterations in the nanocluster structure.

In this work, first-principles calculations were performed to reveal the size effect and the nanoscale mechanism of water molecules above the MAPbI_3 perovskite. Working on three distinct-sized MAPbI_3 nanoclusters, we reveal that there exists a strong band gap opening with reduced size in the perovskite nanoclusters. Through decomposed analysis, for the first time, we discover that the outermost octahedral layer of the perovskite nanocluster protects the integrity of the structure from the water layer while, surprisingly, the subsurface layers undergo more significant deviation from the bulk positions. It is likely that the degradation initiates from those subsurface layers. As subsurface layers of MAPbI_3 nanoclusters undergo the most significant lattice expansion, it is much easier to substitute Pb or I atoms in these subsurface layers for interstitial doping. Adding any surface passivation layer containing different functional ending groups, one with enough affinity of the Pb–I in perovskite to maintain mechanical continuity, while on the other end containing a hydrophobic

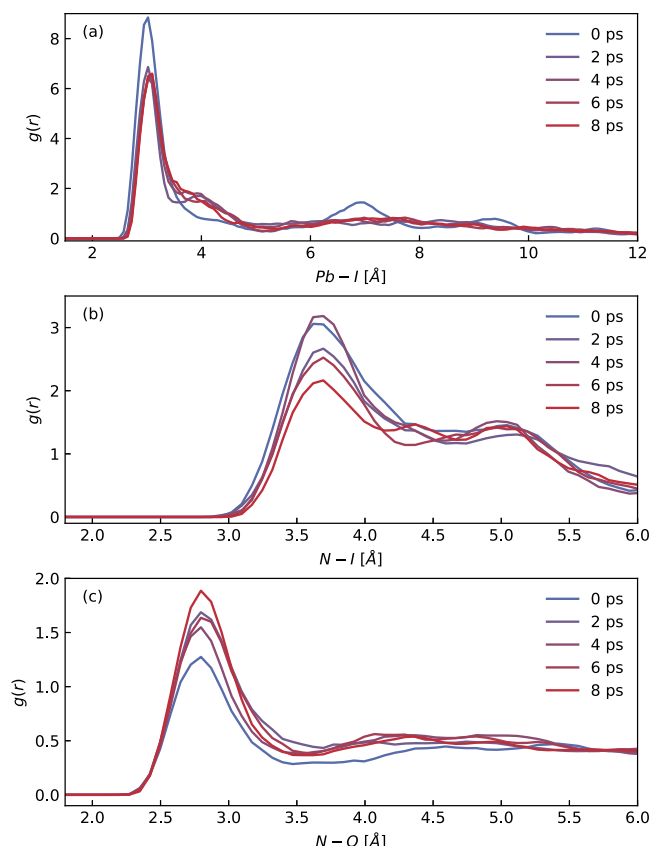


Figure 6. RDFs for Pb–I (a), N–I (b), and N–O (c) for each time window, with a length of 2 ps. (a) The periodic lattice structure is destroyed within the first 4 ps. (b) An increasing number of MA cations are leaving their original positions. (c) Water molecules capture MA cations during the dissolution process.

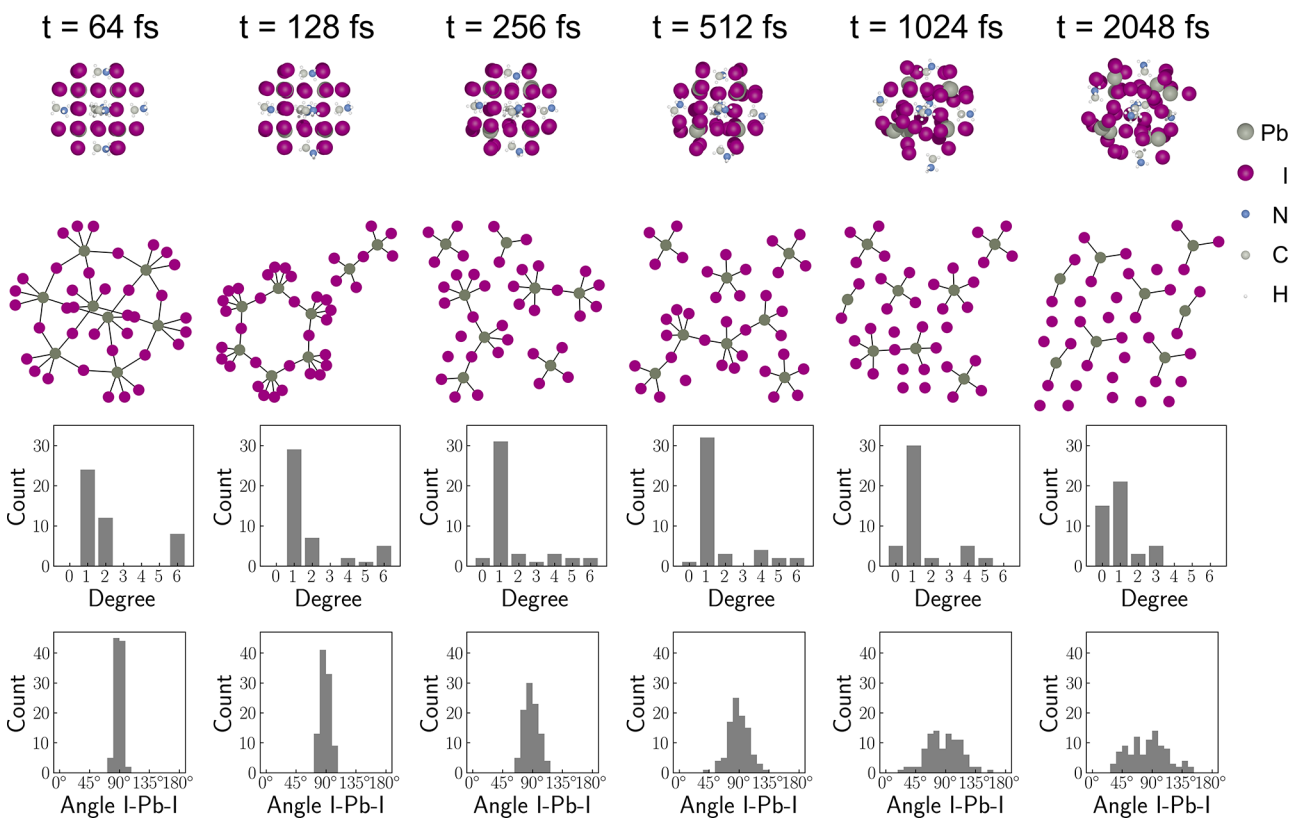


Figure 7. Configurations, graph structures, degree distributions, and angle I–Pb–I distributions for different frames at times 64, 128, 256, 512, 1024, and 2048 fs. The topological connection graph is generated based on the geometric criterion that the Pb–I distance is less than 3.4 Å.

unit to resist the water, would help improve the stability of perovskites.

Importantly, we report the generation of water-induced defective states. Initially localized above the valence top within the band gap for the small-sized nanocluster, the defective states finally evolve into band-like states buried within the whole gap of host MAPbI₃ for the big-sized nanocluster. Our work suggests that water molecules function as dopants and can generate hot-spot-like localized states within the gap. Even a trace of such a residual water molecule will affect light utilization and act as a trapping center for photoinduced carriers.

Furthermore, AIMD simulations show that the small-sized MAPbI₃ nanocluster, as large as the nanocluster examined here, is highly dynamically unstable in water. The MA cations have a tendency to detach from the nanoclusters, being captured by water molecules, which finally leads to instability. Analysis of the time evolution of the breaking of the crystal structure suggests that many Pb–I bonds are broken within 2 ps. Nevertheless, clusters with bigger sizes, endowed with a higher amount of formation enthalpy, may eventually compensate for the increase of entropy and become stabilized in water.

Our work provides a new perspective on the quantum size effect and the critical role of water in the electronic structure and structural evolution of organic perovskite, which will be helpful for designing a water-resistant layer and water-included solvent for the growth of perovskite. Looking ahead, our study could inspire researchers to examine the quantum confinement effect of the perovskite nanocluster and initiate surface modification to enhance resistance to degradation by water. Furthermore, the identification of water-induced defective

states within the band gap suggest compelling needs of measures of removal of these localized states, weak per molecule but massive in total, which is critical for light utilization and promoting photovoltaic efficiency of perovskite solar cells.

ASSOCIATED CONTENT

Supporting Information

The Supporting Information is available free of charge at <https://pubs.acs.org/doi/10.1021/acs.jpcllett.3c02807>.

Adsorption energy calculation details; perovskite–water ratio impact on the MAPbI₃ cluster in both structure and PDOS; and AIMD trajectory analysis including the MAPbI₃ structure evolution and coordination number analysis ([PDF](#))

AUTHOR INFORMATION

Corresponding Author

Yongqing Cai – Joint Key Laboratory of Ministry of Education Institute of Applied Physics and Materials Engineering, University of Macau, Macau, China;
orcid.org/0000-0002-3565-574X; Email: yongqingcai@um.edu.mo

Authors

Jie Huang – Joint Key Laboratory of Ministry of Education Institute of Applied Physics and Materials Engineering, University of Macau, Macau, China
Bowen Wang – Joint Key Laboratory of Ministry of Education Institute of Applied Physics and Materials Engineering, University of Macau, Macau, China

Hejin Yan — Joint Key Laboratory of Ministry of Education
Institute of Applied Physics and Materials Engineering,
University of Macau, Macau, China

Complete contact information is available at:
<https://pubs.acs.org/10.1021/acs.jpclett.3c02807>

Notes

The authors declare no competing financial interest.

ACKNOWLEDGMENTS

This work was financially supported by the Natural Science Foundation of China (Grant 22022309, EF001/IAPME-CYQ/2021/NSFC), the Natural Science Foundation of Guangdong Province, China (2021A1515010024, EF009/IAPME-CYQ/2021/GDSTC), the Science and Technology Development Fund from Macau SAR (0120/2023/RIA2, 0085/2023/ITP2, FDCT-0163/2019/A3), and the University of Macau (MYRG2020-00075-IAPME). This work was conducted on the High-Performance Computing Cluster (HPCC), which is supported by the Information and Communication Technology Office (ICTO) at the University of Macau. Some portions of the calculations were also performed on Triton, provided by the Aalto Science-IT project. J.H. acknowledges Dr. Gang Huang for his insightful discussions.

REFERENCES

- (1) Kojima, A.; Teshima, K.; Shirai, Y.; Miyasaka, T. Organometal halide perovskites as visible-light sensitizers for photovoltaic cells. *J. Am. Chem. Soc.* **2009**, *131*, 6050–6051.
- (2) Ansari, M. I. H.; Qurashi, A.; Nazeeruddin, M. K. Frontiers, opportunities, and challenges in perovskite solar cells: a critical review. *J. Photochem. Photobiol., C* **2018**, *35*, 1–24.
- (3) Yin, T.; Yan, H.; Abdelwahab, I.; Lekina, Y.; Lü, X.; Yang, W.; Sun, H.; Leng, K.; Cai, Y.; Shen, Z. X.; et al. Pressure driven rotational isomerism in 2D hybrid perovskites. *Nat. Commun.* **2023**, *14*, 411.
- (4) Shao, Y.; Gao, W.; Yan, H.; Li, R.; Abdelwahab, I.; Chi, X.; Rogée, L.; Zhuang, L.; Fu, W.; Lau, S. P.; et al. Unlocking surface octahedral tilt in two-dimensional Ruddlesden-Popper perovskites. *Nat. Commun.* **2022**, *13*, 138.
- (5) Kripalani, D. R.; Cai, Y.; Lou, J.; Zhou, K. Strong edge stress in molecularly thin organic-inorganic hybrid ruddlesden-popper perovskites and modulations of their edge electronic properties. *ACS Nano* **2022**, *16*, 261–270.
- (6) Chen, H.; Yan, H.; Cai, Y. Recipe for the design of mixed cation lead halide perovskites: adsorption and charge transfer from A-site cations to PbI₂. *J. Mater. Chem. A* **2023**, *11*, 19349–19359.
- (7) Chen, H.; Guan, Q.; Yan, H.; Cui, X.; Shu, Z.; Cai, Y. Additive molecules adsorbed on monolayer PbI₂: atomic mechanism of solvent engineering for perovskite solar cells. *ACS Appl. Mater. Interfaces* **2023**, *15*, 32475–32486.
- (8) Yan, H.; Wang, B.; Yan, X.; Guan, Q.; Chen, H.; Shu, Z.; Wen, D.; Cai, Y. Efficient passivation of surface defects by lewis base in lead-free tin-based perovskite solar cells. *Materials Today Energy* **2022**, *27*, 101038.
- (9) Chun, F.; Zhang, B.; Li, Y.; Li, W.; Xie, M.; Peng, X.; Yan, C.; Chen, Z.; Zhang, H.; Yang, W. Internally-externally defects-tailored MAPbI₃ perovskites with highly enhanced air stability and quantum yield. *Chem. Eng. J.* **2020**, *399*, 125715.
- (10) Yang, J.; Kelly, T. L. Decomposition and cell failure mechanisms in lead halide perovskite solar cells. *Inorg. Chem.* **2017**, *56*, 92–101.
- (11) Chowdhury, T. A.; Bin Zafar, M. A.; Sajjad-Ul Islam, M.; Shahinuzzaman, M.; Islam, M. A.; Khandaker, M. U. Stability of perovskite solar cells: issues and prospects. *RSC Adv.* **2023**, *13*, 1787–1810.
- (12) Boyd, C. C.; Cheacharoen, R.; Leijtens, T.; McGehee, M. D. Understanding degradation mechanisms and improving stability of perovskite photovoltaics. *Chem. Rev.* **2019**, *119*, 3418–3451.
- (13) Eperon, G. E.; Habreutinger, S. N.; Leijtens, T.; Bruijnaers, B. J.; van Franeker, J. J.; deQuilettes, D. W.; Pathak, S.; Sutton, R. J.; Grancini, G.; Ginger, D. S.; et al. The importance of moisture in hybrid lead halide perovskite thin film fabrication. *ACS Nano* **2015**, *9*, 9380–9393.
- (14) Yang, S.; Wang, Y.; Liu, P.; Cheng, Y.-B.; Zhao, H. J.; Yang, H. G. Functionalization of perovskite thin films with moisture-tolerant molecules. *Nat. Energy* **2016**, *1*, 15016.
- (15) Lv, Q.; He, W.; Lian, Z.; Ding, J.; Li, Q.; Yan, Q. Anisotropic moisture erosion of CH₃NH₃PbI₃ single crystals. *CrystEngComm* **2017**, *19*, 901–904.
- (16) Wen, T. Y.; Yang, S.; Liu, P. F.; Tang, L. J.; Qiao, H. W.; Chen, X.; Yang, X. H.; Hou, Y.; Yang, H. G. Surface electronic modification of perovskite thin film with water-resistant electron delocalized molecules for stable and efficient photovoltaics. *Adv. Energy Mater.* **2018**, *8*, 1703143.
- (17) Noh, J. H.; Im, S. H.; Heo, J. H.; Mandal, T. N.; Seok, S. I. Chemical management for colorful, efficient, and stable inorganic-organic hybrid nanostructured solar cells. *Nano Lett.* **2013**, *13*, 1764–1769.
- (18) Frost, J. M.; Butler, K. T.; Brivio, F.; Hendon, C. H.; van Schilfgaarde, M.; Walsh, A. Atomistic origins of high-performance in hybrid halide perovskite solar cells. *Nano Lett.* **2014**, *14*, 2584–2590.
- (19) Leguy, A. M. A.; Hu, Y.; Campoy-Quiles, M.; Alonso, M. I.; Weber, O. J.; Azarhoosh, P.; van Schilfgaarde, M.; Weller, M. T.; Bein, T.; Nelson, J.; et al. Reversible hydration of CH₃NH₃PbI₃ in films, single crystals, and solar cells. *Chem. Mater.* **2015**, *27*, 3397–3407.
- (20) Han, Y.; Meyer, S.; Dkhissi, Y.; Weber, K.; Pringle, J. M.; Bach, U.; Spiccia, L.; Cheng, Y.-B. Degradation observations of encapsulated planar CH₃NH₃PbI₃ perovskite solar cells at high temperatures and humidity. *J. Mater. Chem. A* **2015**, *3*, 8139–8147.
- (21) Niu, G.; Guo, X.; Wang, L. Review of recent progress in chemical stability of perovskite solar cells. *J. Mater. Chem. A* **2015**, *3*, 8970–8980.
- (22) Song, Z.; Abate, A.; Watthage, S. C.; Liyanage, G. K.; Phillips, A. B.; Steiner, U.; Graetzel, M.; Heben, M. J. Perovskite solar cell stability in humid air: partially reversible phase transitions in the PbI₂-CH₃NH₃I-H₂O system. *Adv. Energy Mater.* **2016**, *6*, 1600846.
- (23) Sun, P.-P.; Chi, W.-J.; Li, Z.-S. Effects of water molecules on the chemical stability of MAGeI₃ perovskite explored from a theoretical viewpoint. *Phys. Chem. Chem. Phys.* **2016**, *18*, 24526–24536.
- (24) Zhu, Z.; Hadjiev, V. G.; Rong, Y.; Guo, R.; Cao, B.; Tang, Z.; Qin, F.; Li, Y.; Wang, Y.; Hao, F.; et al. Interaction of organic cation with water molecule in perovskite MAPbI₃: from dynamic orientational disorder to hydrogen bonding. *Chem. Mater.* **2016**, *28*, 7385–7393.
- (25) Varadwaj, A.; Varadwaj, P. R.; Yamashita, K. Hybrid organic-inorganic CH₃NH₃PbI₃ perovskite building blocks: Revealing ultrastrong hydrogen bonding and mulliken inner complexes and their implications in materials design. *J. Comput. Chem.* **2017**, *38*, 2802–2818.
- (26) Radicchi, E.; Mosconi, E.; Elisei, F.; Nunzi, F.; De Angelis, F. Understanding the solution chemistry of lead halide perovskites precursors. *ACS Appl. Energy Mater.* **2019**, *2*, 3400–3409.
- (27) Radicchi, E.; Ambrosio, F.; Mosconi, E.; Alasmari, A. A.; Alasmari, F. A. S.; De Angelis, F. Combined computational and experimental investigation on the nature of hydrated iodoplumbate complexes: insights into the dual role of water in perovskite precursor solutions. *J. Phys. Chem. B* **2020**, *124*, 11481–11490.
- (28) Liu, D.; Traverse, C. J.; Chen, P.; Elinski, M.; Yang, C.; Wang, L.; Young, M.; Lunt, R. R. Aqueous-Containing Precursor Solutions for Efficient Perovskite Solar Cells. *Adv. Sci.* **2018**, *5*, 1700484.
- (29) Geng, C.; Xu, S.; Zhong, H.; Rogach, A. L.; Bi, W. Aqueous Synthesis of Methylammonium Lead Halide Perovskite Nanocrystals. *Angew. Chem., Int. Ed.* **2018**, *57*, 9650–9654.

- (30) Mosconi, E.; Azpiroz, J. M.; De Angelis, F. Ab initio molecular dynamics simulations of methylammonium lead iodide perovskite degradation by water. *Chem. Mater.* **2015**, *27*, 4885–4892.
- (31) Bass, K. K.; McAnally, R. E.; Zhou, S.; Djurovich, P. I.; Thompson, M. E.; Melot, B. C. Influence of moisture on the preparation, crystal structure, and photophysical properties of organohalide perovskites. *Chem. Commun.* **2014**, *50*, 15819–15822.
- (32) Zhou, H.; Chen, Q.; Li, G.; Luo, S.; Song, T.-b.; Duan, H.-S.; Hong, Z.; You, J.; Liu, Y.; Yang, Y. Interface engineering of highly efficient perovskite solar cells. *Science* **2014**, *345*, 542–546.
- (33) Li, J.; Dobrovolsky, A.; Merdasa, A.; Unger, E. L.; Scheblykin, I. G. Luminescent intermediates and humidity-dependent room-temperature conversion of the MAPbI₃ Perovskite Precursor. *ACS Omega* **2018**, *3*, 14494–14502.
- (34) Huang, J.; Tan, S.; Lund, P. D.; Zhou, H. Impact of H₂O on organic-inorganic hybrid perovskite solar cells. *Energy Environ. Sci.* **2017**, *10*, 2284–2311.
- (35) Contreras-Bernal, L.; Aranda, C.; Valles-Pelarda, M.; Ngo, T. T.; Ramos-Terrón, S.; Gallardo, J. J.; Navas, J.; Guerrero, A.; Mora-Seró, I.; Idígoras, J.; et al. Homeopathic perovskite solar cells: effect of humidity during fabrication on the performance and stability of the device. *J. Phys. Chem. C* **2018**, *122*, 5341–5348.
- (36) Petrus, M. L.; Hu, Y.; Moia, D.; Calado, P.; Leguy, A. M. A.; Barnes, P. R. F.; Docampo, P. The influence of water vapor on the stability and processing of hybrid perovskite solar cells made from non-stoichiometric precursor mixtures. *ChemSusChem* **2016**, *9*, 2699–2707.
- (37) Liu, K.; Luo, Y.; Jin, Y.; Liu, T.; Liang, Y.; Yang, L.; Song, P.; Liu, Z.; Tian, C.; Xie, L.; et al. Moisture-triggered fast crystallization enables efficient and stable perovskite solar cells. *Nat. Commun.* **2022**, *13*, 4891.
- (38) Hjorth Larsen, A.; Jørgen Mortensen, J.; Blomqvist, J.; Castelli, I. E.; Christensen, R.; Dulak, M.; Friis, J.; Groves, M. N.; Hammer, B.; Hargus, C.; et al. The atomic simulation environment—a Python library for working with atoms. *J. Phys.: Condens. Matter* **2017**, *29*, 273002.
- (39) Bahn, S. R.; Jacobsen, K. W. An object-oriented scripting interface to a legacy electronic structure code. *Comput. Sci. Eng.* **2002**, *4*, 56–66.
- (40) Kühne, T. D.; Iannuzzi, M.; Del Ben, M.; Rybkin, V. V.; Seewald, P.; Stein, F.; Laino, T.; Khaliullin, R. Z.; Schütt, O.; Schiffmann, F.; et al. CP2K: An electronic structure and molecular dynamics software package - quickstep: efficient and accurate electronic structure calculations. *J. Chem. Phys.* **2020**, *152*, 194103.
- (41) Hartwigsen, C.; Goedecker, S.; Hutter, J. Relativistic separable dual-space Gaussian pseudopotentials from H to Rn. *Phys. Rev. B* **1998**, *58*, 3641–3662.
- (42) Lippert, G.; Hutter, J.; Parrinello, M. The Gaussian and augmented-plane-wave density functional method for ab initio molecular dynamics simulations. *Theor. Chem. Acc.* **1999**, *103*, 124–140.
- (43) Perdew, J. P.; Burke, K.; Ernzerhof, M. Generalized gradient approximation made simple. *Phys. Rev. Lett.* **1996**, *77*, 3865–3868.
- (44) Grimme, S.; Antony, J.; Ehrlich, S.; Krieg, H. A consistent and accurate ab initio parametrization of density functional dispersion correction (DFT-D) for the 94 elements H–Pu. *J. Chem. Phys.* **2010**, *132*, 154104.
- (45) Broyden, C. G. The convergence of a class of double-rank minimization algorithms 1. general considerations. *IMA J. Appl. Math.* **1970**, *6*, 76–90.
- (46) Fletcher, R. A new approach to variable metric algorithms. *Comput. J.* **1970**, *13*, 317–322.
- (47) Goldfarb, D. A family of variable-metric methods derived by variational means. *Math. Comput.* **1970**, *24*, 23–26.
- (48) Shanno, D. F. Conditioning of quasi-Newton methods for function minimization. *Math. Comput.* **1970**, *24*, 647–656.
- (49) Liu, D. C.; Nocedal, J. On the limited memory BFGS method for large scale optimization. *Math. Program.* **1989**, *45*, 503–528.
- (50) Martyna, G. J.; Klein, M. L.; Tuckerman, M. Nosé-Hoover chains: The canonical ensemble via continuous dynamics. *J. Chem. Phys.* **1992**, *97*, 2635–2643.
- (51) Michaud-Agrawal, N.; Denning, E. J.; Woolf, T. B.; Beckstein, O. MDAnalysis: A toolkit for the analysis of molecular dynamics simulations. *J. Comput. Chem.* **2011**, *32*, 2319–2327.
- (52) Gowers, R. J.; Linke, M.; Barnoud, J.; Reddy, T. J. E.; Melo, M. N.; Seyler, S. L.; Domański, J.; Dotson, D. L.; Buchoux, S.; Kenney, I. M. MDAnalysis: a Python package for the rapid analysis of molecular dynamics simulations. *Proceedings of the 15th Python in science conference*; U.S. Department of Energy, Office of Scientific and Technical Information: 2016; pp 98–105.
- (53) Jahn, H. A.; Teller, E. Stability of polyatomic molecules in degenerate electronic states - I—Orbital degeneracy. *Proc. R. Soc. A* **1937**, *161*, 220–235.
- (54) Yang, J.; Yuan, Z.; Liu, X.; Braun, S.; Li, Y.; Tang, J.; Gao, F.; Duan, C.; Fahlman, M.; Bao, Q. Oxygen- and water-induced energetics degradation in organometal halide perovskites. *ACS Appl. Mater. Interfaces* **2018**, *10*, 16225–16230.